



Human Hepatocellular Carcinoma Metabolism: Imaging by Hyperpolarized ^{13}C Magnetic Resonance Spectroscopy

Moses M. Darpolor^{1*}, David E. Kaplan², Peter L. Pedersen³ and Jerry D. Glickson¹

Abstract

Purpose: Most cancers exhibit high levels of aerobic glycolytic metabolism with diminished levels of mitochondrial oxidative phosphorylation even in the presence of normal or near-normal levels of oxygen (“Warburg effect”). However, technical challenges have limited the development of non-invasive *in vivo* imaging techniques for monitoring glycolytic metabolism of hepatocellular carcinoma (HCC) and quantitatively evaluating the impact of this effect on the growth and therapy of this disease. Thus, there is a critical need to develop non-invasive techniques for longitudinal assessment of the metabolism and treatment response of patients with unresectable HCCs.

Procedures: This article discusses a novel method, “Hyperpolarized ^{13}C MRS imaging”, for achieving this objective and thus improving the prognosis of HCC patients. The primary objective has been to characterize *in vivo* metabolic biomarkers as determinants of HCC metabolism and treatment response of unresectable HCC tumors or viable HCC cells.

Results: This innovative technique capitalizes on a new technology that increases the sensitivity of MRS detection of crucial metabolites in cancer cells.

Conclusion: It is anticipated that this innovative approach will lead to improved methods, both for the diagnosis and staging of HCCs and for the facilitation of the development of enzyme targeted therapies and other therapeutic interventions.

Keywords: Hepatocellular Carcinoma, “Warburg effect”, Hyperpolarized ^{13}C MRS, [^{13}C] pyruvate, Alanine Transaminase, Branched-Chain Aminotransferases

Abbreviations: HCC: Hepatocellular Carcinoma; MRSI: Magnetic Resonance Spectroscopic Imaging; ATP: Adenine Triphosphate; TCA: Tricarboxylic Acid; DNP: Dynamic Nuclear Polarization; NAD(P)H: Nicotinamide Adenine (phosphate) dinucleotide; LDH-A: Lactate Dehydrogenase A; HBV: Hepatitis B Virus; HCV: Hepatitis C Virus; 3D DSE-EPSI: Three-dimensional double-spin-echo echo-planar

*Corresponding author: Moses M. Darpolor, PhD, University of Pennsylvania, Department of Radiology, B-6 Blockley Hall - 6021, 423 Guardian Drive, Philadelphia, PA 19104-6100, USA, E-mail: mdarpolor@gmail.com

Received: July 13, 2012 Accepted: August 28, 2012 Published: August 31, 2012

spectroscopic imaging; PCR: Polymerase Chain Reaction; NQO1: NAD(P)H Dehydrogenase Quinone 1; ALT: Alanine Transaminase; SEM: Standard Error of Mean; BCAT-1 or -2: Branched-Chain Aminotransferases-1 or -2; cDNA: Complementary Deoxyribonucleic Acid; TACE: Transcatheter Arterial Chemoembolization.

Introduction

A characteristic feature of cancer cells is the alteration of their central carbon metabolism. It is generally acknowledged that for energy production cancer cells enhance their utilization of glycolysis and diminish that of oxidative phosphorylation irrespective of oxygen supply [1]. However, although mechanistic explanations for this enhanced glycolytic phenotype are controversial, it is likely due to the need for a versatile method for ATP production to serve as a direct form of energy, or as energy to drive both biosynthesis of vital intermediates for cell growth and provide anaplerotic flux for the tricarboxylic acid (TCA) cycle [2-4].

As technological improvements increase the feasibility of studying cancer metabolism, a growing number of reports have investigated the molecular basis of malignant transformation and cell metabolism. Recently, a state-of-the-art metabolome analysis tool based on capillary electrophoresis coupled to mass spectrometry [5] quantified the various levels of metabolites involved in central carbon metabolism in human tumor tissues and globally mapped the glycolysis, pentose phosphate, and TCA pathways. In addition, the liquid state preservation of polarized nuclear spins from dynamic nuclear polarization (DNP) [6] has advanced ^{13}C magnetic resonance spectroscopic imaging (MRSI) and enabled the implementation of *in vivo* tumor metabolic imaging with hyperpolarized [^{13}C] pyruvate [7-15], ^{13}C -labelled bicarbonate [16], [^{13}C]fructose [17], [^{13}C]fumarate [18] or [^{13}C]ketoisocaproate [19] to investigate local changes in the carbon metabolic pathways after intravenous administration of the hyperpolarized substrate. Detection of these substrates and their metabolic products provide crucial information about multiple transporters and enzymes involved in carbon metabolism. Due to the short lifetime of the hyperpolarized signal (~60 s), a complete investigation of carbon metabolism is not feasible in a single data acquisition session.

Hyperpolarized [^{13}C]pyruvate MRSI was previously used to demonstrate changes in metabolism of fasted rat liver in which the [^{13}C]lactate to [^{13}C]alanine ratios increased as compared to normal rat liver [20]. Another study demonstrated an increased lactate production rate in rat liver when [^{13}C]pyruvate was co-administered with ethanol [21]. This finding was attributed to increase nicotinamide adenine dinucleotide (NADH) in relation to ethanol metabolism in the rat liver. More recently, it was reported that a fasted rat bearing an orthotopic HCC showed increased [^{13}C]lactate and [^{13}C]alanine levels after a bolus intravenous injection of hyperpolarized [^{13}C]pyruvate [15]. Unlike most [^{13}C]pyruvate studies, a single-voxel MRS study [15] and a MRS imaging study [9] revealed a marked increase in [^{13}C]alanine above that from [^{13}C]lactate in tumors. A switchable transgenic mouse model of MYC-driven liver cancer showed a correlation of increased alanine to tumor formation and increased lactate as a biomarker [22]. However, a seminar review

[23] discussed that the glycolytic phenotype observed in tumor cells is regulated by the PI3K, hypoxia-inducible factor (HIF), p53, MYC and AMP-activated protein kinase (AMPK)-liver kinase B1 (LKB1) pathways, which make it difficult to attribute the glycolytic phenotype of liver cancer to a single pathway. These contributions are significant because they may characterize inherent biomarkers of HCC that can provide new insights into the progression of unresectable hepatomas. Studies have previously investigated the pattern of glycolytic enzymes in buffalo rat hepatomas using invasive tissue assay analyses [24, 25]. With the exceptions of glucokinase, phosphofructokinase and pyruvate kinase, the activities of the enzymes of the main glycolytic pathway are generally similar in rat liver and hepatomas [25]. The activities of these three enzymes, glucokinase, phosphofructokinase and pyruvate kinase, reflect the growth potential of the tumors that is consistently highest in the more rapidly growing HCC tumors and gradually decreasing from slowly growing HCC tumors to normal rat liver.

The enzyme patterns of rat hepatomas also showed distinctive changes indirectly related to glycolysis at branched points that involve alternate pathways to the main glycolytic route. One such pathway is *via* lactate dehydrogenase (LDH). The ratio of LDH to glycerol phosphate dehydrogenase activities was highest in the most rapidly growing HCC tumors and lowest in the slowly growing HCC tumors as compared to normal liver, thereby suggesting a correlation of the rate of aerobic glycolysis of malignant tissues to their rate of proliferation. Also, it has been noted that total tyrosine aminotransferase in many host livers and hepatomas were slightly elevated in rats fed a vitamin B₆-deficient diet [24]. These observations could point to distinguishable metabolic markers of HCC that may be identifiable *in vivo*. In light of these findings, we conclude that previous studies have not adequately investigated enzyme levels in connection with catalyzed metabolites in *in vivo* HCC animal models or in humans.

Liver cancer, the vast majority (91%) of which is hepatocellular carcinoma (HCC), is the sixth most common cancer worldwide, and the third most common cause of death from cancer [26]. The incidence rates of HCC tripled in the United States from 1975 through 2005 across all ethnic groups with marked recent increases among middle-aged black, hispanic, and white males [27]. The rapid increases in HCC incidence in developed countries correlates with a similar trend in the prevalence of chronic infection with hepatitis B virus (HBV) [27,28] and hepatitis C virus (HCV) [27,29]. Most patients with HCC are diagnosed when the disease is already at an advanced stage, thereby limiting therapeutic options and leading to a dismal one-year cause-specific survival rate [27]. This health challenge warrants efforts to effectively manage and treat the disease. Research on alterations of gene and protein expression of HCC could facilitate identification of molecular hallmarks for effective therapeutic strategies. Therefore, suitable animal models of orthotopic HCC that permits the control of genetic and environmental conditions in longitudinal studies promises to recapitulate all phases of the disease, facilitate the development of diagnostic or prognostic biomarkers, develop robust tumor imaging approaches, and provide evaluation of potential therapeutic strategies. Perhaps, limited technologies may have previously prevented initiation of advanced imaging studies of HCC metabolism *in vivo* with subsequent translation into humans. There is clearly a critical need for introduction of robust technologies to permit earlier intervention and provide better

prognosis. Researchers may develop measures for distinguishing the metabolic characteristics of HCC and identify promising therapeutic modalities for improving studies of HCC metabolism. The expected outcomes may be utilized complementarily for down-staging of HCC to meet established criteria for liver transplantation and for assessing functional hepatic reserve. In addition, the early detection of treatment failure will permit other treatment options thus avoiding wasted time, cost and morbidity. Furthermore, better understanding of the metabolic phenotype of HCC could lead to pharmacologic strategies that may develop targeted inhibition of crucial enzymes in the inherent biochemical pathway(s) of HCC.

Materials and Methods

In vivo Hyperpolarized ¹³C MRS Imaging

A total of 7 male buffalo rats (Charles River Laboratories International Inc., Wilmington, MA) were used in this study. All procedures with animals were performed in accordance with the recommendations in the guide for the Care and Use of Laboratory Animals of the National Institutes of Health, and the protocol was approved by the Institutional Animal Care and Use Committee (IACUC). During single orthotopic implantation, a subxiphoid incision was made and a total of 1×10⁶ Morris hepatoma McA-RH7777 cells (American Type Culture Collection, Manassas, VA) suspended in 100 μL of phosphate-buffered saline (PBS) were injected slowly (typically over 15-30 seconds) beneath the parenchyma of the middle lobe. At 12 to 14 days post-implantation, this cohort of rats (N=7) was treated on two consecutive days with a doxorubicin HCl liposome injection, Doxil[®] (2.5 mg/kg, intraperitoneally, i.p.), (Ben Venue Laboratories Inc, Bedford, OH) prior to hyperpolarized ¹³C MRSI. Experiments were performed on rats anesthetized with 2% isoflurane in oxygen at a flow rate of 1.5 L/min. An MR-compatible small animal monitoring and gating system (Model 1025, SA Instruments Inc., Stony Brook, NY) was used to measure and record physiological parameters of each rat. A custom-built dual-tuned (¹H/¹³C) quadrature rat coil was used for both radiofrequency (RF) transmission and reception in a 3.0 Tesla clinical system (Signa[™] MR Scanner, GE Healthcare, Waukesha, WI). An 8 molar ¹³C-urea phantom was placed alongside each rat for experimental calibrations. A mixture of [1-¹³C]pyruvic acid and trityl radical was polarized to approximately 23.7±1.7% using a DNP polarizer (HyperSense[™], Oxford Instruments Molecular Biotools, Oxford, UK). After the mixture was polarized for 1 hour, it was rapidly dissolved using a Tris/EDTA NaOH buffer (pH=7.5±0.1). A 3 mL bolus injection of hyperpolarized [1-¹³C]pyruvate (80 mM) was administered *via* the tail vein over a 14 s interval followed by a 4 s saline flush to clear the 0.5 mL catheter dead volume. A 3D DSE-EPSI sequence [30] was utilized, which allows a maximum in-plane spatial resolution of 3.4 mm with spectral bandwidth (BW) of 500 Hz to include the metabolite peaks. A 30 mm axial slab was excited to cover the rat liver. Hyperpolarized [1-¹³C]ketoisocaproate (KIC) technique was performed as previously published [19] with an axial slab (4 mm) across the liver, a tail vein injection of 2.7 mL of 23 mM KIC, and 5° flip angle acquisitions in dynamic spiral CSI [31]. Data reconstruction and analysis were performed using custom software written in Matlab (The MathWorks, Inc., Natick, MA, USA).

Quantitative real-time PCR analysis

Following the MRSI examinations of 4 rats, rat liver tissues were harvested and immediately snap-frozen in cold acetone and stored

at -80°C . About 30 mg of snap-frozen tissue was used from each rat specimen to extract mRNA. Total RNA enriched with mRNA was purified with RNeasy Mini Kit (Qiagen, Valencia, CA). All procedures were performed according to the manufacturers' recommendations. Following a 1:50 dilution of samples, aliquots were pipetted into microplate wells and absorbance at 260 nm was measured using a PowerWave™ XS Microplate Spectrophotometer (BioTek Instruments, Winooski, VT). Reverse transcription (RT) using 500 ng of total RNA in a 10 μL reaction was performed using the Applied Biosystems RT Kit (Applied Biosystems, Foster City, CA) according to the instruction manual. Synthesized cDNA was then maintained at 37°C for 1 h, followed by 10 min at 95°C . cDNA was PCR-amplified in a 20- μL reaction using the TaqMan® Gene Expression Assay Kit and Master Mix Kit (Applied Biosystems, Foster City, CA) according to the instruction manual. Briefly, thermal cycling was performed using the Mx3000P real-time PCR system (Stratagene®, Santa Clara, CA), amplification rates were measured automatically, and the number of cycles needed to cross the threshold (C_t) determined. Each sample was assayed in triplicates for levels of both cytosolic and mitochondrial branched-chain aminotransferases (BCAT-1 and BCAT-2). The mRNA from Morris hepatoma McA-RH7777 cells, used for tumor implantation, was used to generate standard curves for each enzyme assay. C_t values of respective enzymes were normalized to a reference/housekeeping gene (18S rRNA) as endogenous control. Negative controls included a sample without enzyme in the RT reaction and another sample without template during the PCR.

Statistical analysis

Statistical analysis was performed using GraphPad Prism version 5.0d for Mac OS X (GraphPad Software, San Diego, California, USA). A two-tailed unpaired student's t test was performed to verify the statistical significance of the means in the compared groups. A p-value ≤ 0.05 was considered statistically significant. All results are displayed as mean \pm SEM (standard error of mean) of measures in groups.

Results

Proton MR images (Figure 1) and metabolic maps (Figure

2) of $[1-^{13}\text{C}]$ pyruvate, $[1-^{13}\text{C}]$ lactate, and $[1-^{13}\text{C}]$ alanine from a representative rat are shown. These maps are color-coded with values ranging from minimum (blue) to maximum (red). It is notable that both $[1-^{13}\text{C}]$ lactate and $[1-^{13}\text{C}]$ alanine maps are co-localized with the HCC tumor, and the heterogeneous tumor values are greater than those of normal liver (Figure 2). Spectra from reconstructed voxels in tumor and normal liver are shown (Figure 3a). The integral values of four reconstructed voxels per region (tumor or normal) were tabulated across 7 rats for statistical comparisons (Figure 3b). Each metabolite peak integral was expressed as a ratio to the reference ^{13}C -urea phantom, always placed alongside each rat. There was no significant difference ($p > 0.05$) between the levels of alanine and lactate metabolites in Doxil® treated tumors as compared to those of control rats previously published. In addition, we found a significant upregulation of both cytosolic and mitochondrial branched-chain aminotransferases (BCAT-1 and BCAT-2) in rat HCC tissues (Figure 4) as compared to normal rat tissues. Since these BCAT enzymes indicate strong correlates to those of human HCC tissues, it could be possible to image the activity of these enzymes with hyperpolarized $[1-^{13}\text{C}]$ ketoisocaproate MRS imaging. This technique was demonstrated in rat livers (Figure 5) by implementing a 3D spiral chemical shift imaging [31] pulse sequence.

Discussion

In the study discussed herein, we emphasized the utility of hyperpolarized ^{13}C MRS imaging to measure metabolic signatures of hepatocellular carcinoma. The conversion of pyruvate to lactate and alanine was not significantly affected with Doxil® treatment used in this study. To account for the observed elevated levels of metabolites in HCC tumors, quantitative real-time PCR [9] was used to measure the expression levels of putative enzymes (*LDH-A*, *NQO1*, and *ALT*) associated with the metabolism of $[1-^{13}\text{C}]$ pyruvate. Measurements were made in triplicates for each specimen (tumor or normal liver) from four rats. All three enzymes, LDH-A, NQO1, and ALT were significantly elevated in HCC tumors relative to normal liver tissues.

Using cDNA microarrays to characterize human HCC, another study found an upregulation of BCAT-2 enzymes [32]. It has been

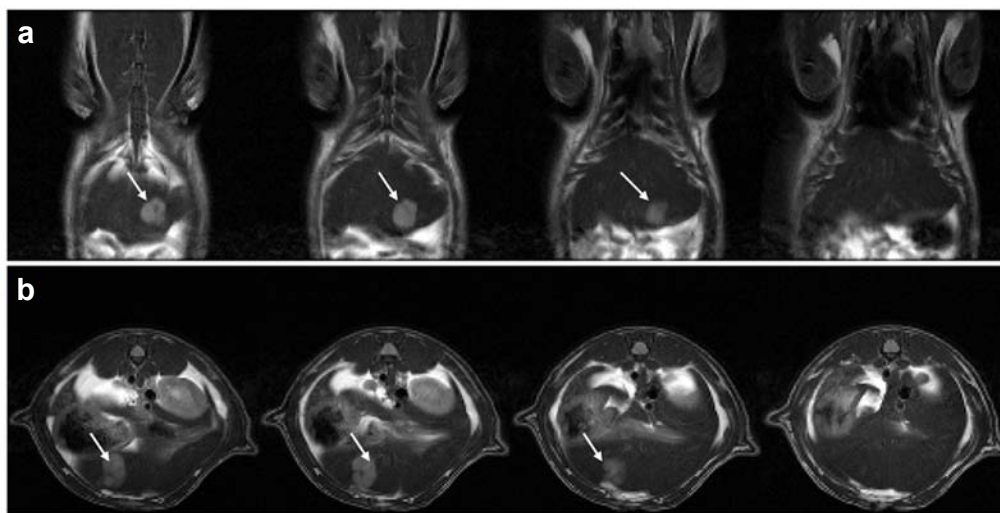
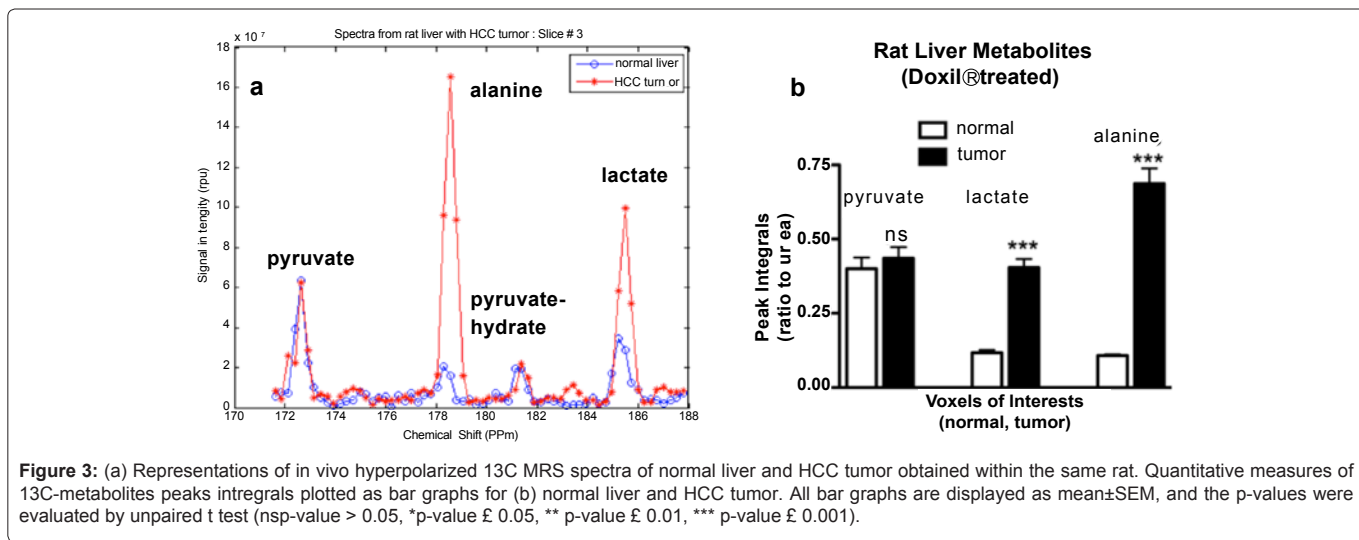
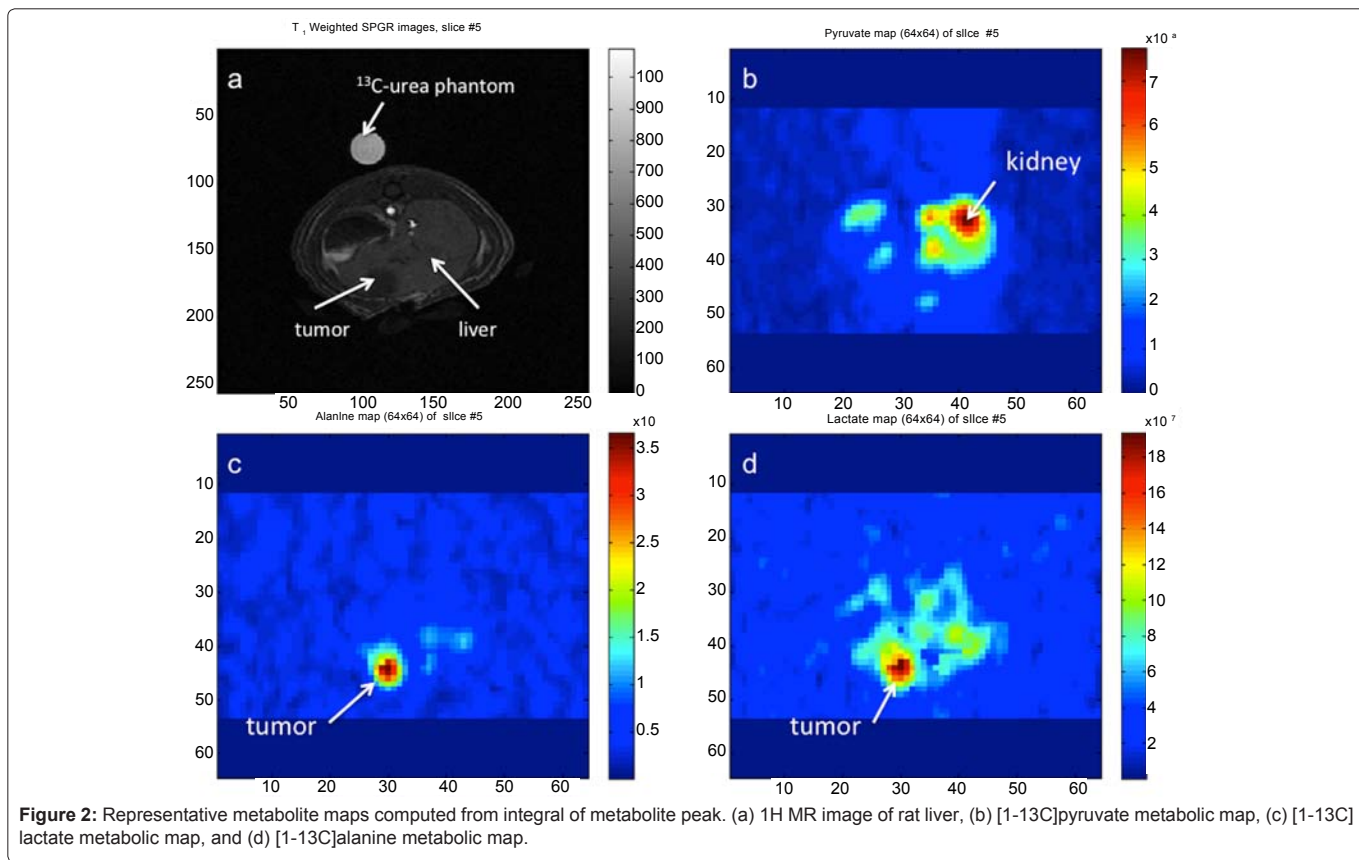


Figure 1: Representative 7T MR images of rat liver at pre-screening with a set of (a) coronal images and (a) axial images with HCC tumors indicated by arrows. A T2-weight fast-spin-echo acquisition, 5 \times 5 cm field-of-view, 256 \times 256 matrix dimensions, and 2 mm slice thickness. [In: Proceedings of the World Molecular Imaging Congress (WMIC); 2010 September 8-11 Abstract# 0049; International Conference Center (ICC), Kyoto, Japan.]



reported that BCAT is only expressed in extra hepatic tissues, and BCAT-2 activity is required in hepatocytes under conditions of rapid cell proliferation [33]. We suspect that ALT and BCAT-1 in the cytoplasm may be associated with the significantly high levels of alanine in HCC, because both enzymes are aminotransferases located in the cytoplasm that transfer the amine group from glutamate to a keto-carbon of an alpha ketoacid like pyruvate. An ongoing study will test this hypothesis with the utility of hyperpolarized [1-¹³C] ketoisocaproate MRSI similar to a recent study on EL4 lymphoma in the mouse [19]. These findings may suggest potential molecular

signatures of HCC, and fortunately, *in vivo* hyperpolarized ¹³C MRS imaging can be used to investigate the catalyzed reactions of the aforementioned enzymes. In addition, this study was performed on a clinical 3 Tesla magnet thereby making the technique translatable into humans with appropriate radio-frequency coil for imaging human livers.

The effect of 3-bromopyruvate on AS-30D rat HCC [34] has shown remarkable results by regressing the tumor completely. The mechanism of 3-bromopyruvate is assumed to inhibit hexokinase

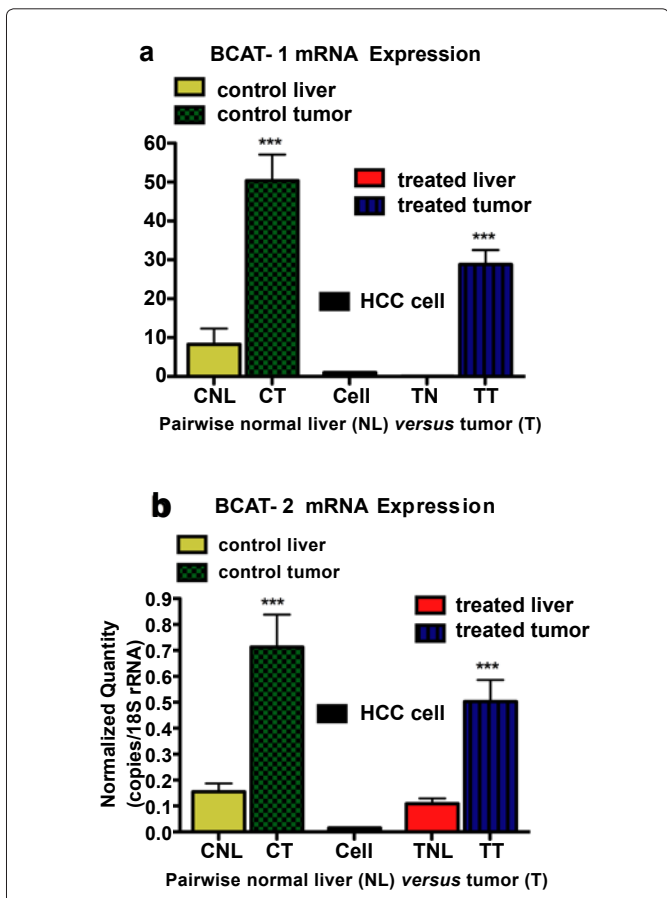


Figure 4: Pairwise bar graphs of enzyme gene expression from normal liver and tumor tissues in control and treated cohorts. (a) branched-chain aminotransferase-1 (BCAT-1) gene expressions, and (b) branched-chain aminotransferase-2 (BCAT-2) gene expressions. All bar graphs are displayed as mean ± SEM, and the p-values were evaluated by unpaired t test (*p-value £ 0.05, ** p-value £ 0.01, *** p-value £ 0.001).

II and prevent glucose from entering the glycolytic pathway [35-38]. More specifically, it is suggested that 3-bromo-pyruvate targets the sulfhydryl group of cysteine residues in hexokinase II [39]. It is possible to label the C1 position with the ^{13}C isotope, 3-bromo-[1- ^{13}C]pyruvate, and hyperpolarize this compound for the study of its

pharmacokinetics and pharmacodynamics. In addition, the spatial distribution of this therapeutic agent could be evaluated with 3D MRS imaging. Another pharmacologic strategy [3] had used small interfering RNA against lactate dehydrogenase to preferentially inhibit the glycolysis of cancer cells. To avoid complications with systemic administration of such a drug *in vivo*, short hairpin RNA can be incorporated into a transcatheter arterial chemoembolization (TACE) to localize the drug within the tumor. As a demonstration of feasibility, image-guided nanoembolization has been performed in a rabbit model of liver cancer to target micro RNA [40]. Other investigators have used ethyl-bromopyruvate, a hydrophobic derivative of 3-bromopyruvate, for intraarterial treatment of a rabbit HCC model (VX2 carcinoma) by a transfemoral intraarterial approach [41].

Potential for clinical translation of hyperpolarized ^{13}C MRSI

Hyperpolarized ^{13}C 3D MRSI is currently limited to preclinical studies. These studies may have overestimated the physiological levels of metabolites because the exogenous metabolic substrate surpasses physiological levels when administered *in vivo*. However, advanced techniques in mass spectrometry have demonstrated elevated levels of lactate and alanine in *ex vivo* human tumors at physiological levels [5]. Despite these limitations, the findings herein strongly support the advent of novel *in vivo* imaging technologies that hold promise for improved diagnosis and prognosis of HCC. MRS imaging could complement retrospective metabolomics of glycolytic metabolites in human HCC tissues with advanced techniques in mass spectrometry as demonstrated in *ex vivo* human tumors [5] and mouse livers [42]. In addition, enzyme analysis can be utilized to validate the translational capabilities of hyperpolarized ^{13}C MRS imaging into humans. In terms of administration of pyruvate, intracoronary pyruvate injections have been successfully performed on clinical patients with congested heart failure (27.75 mmol of pyruvate, 185 mL volume, 15 min injection time) [43,44]. Similarly, this amount of stable isotopic ^{13}C -enriched pyruvate can be hyperpolarized and injected *via* transcatheter arterial infusion as performed on patients with HCC with the advantage of localizing the substrate to the HCC lesion in the liver. However, fast imaging techniques are critical to follow dynamic metabolic processes *in vivo*. Therefore, we encourage researchers to develop fast volumetric ^{13}C MRSI methods for dynamic metabolic imaging. Additionally, the development of novel kinetic

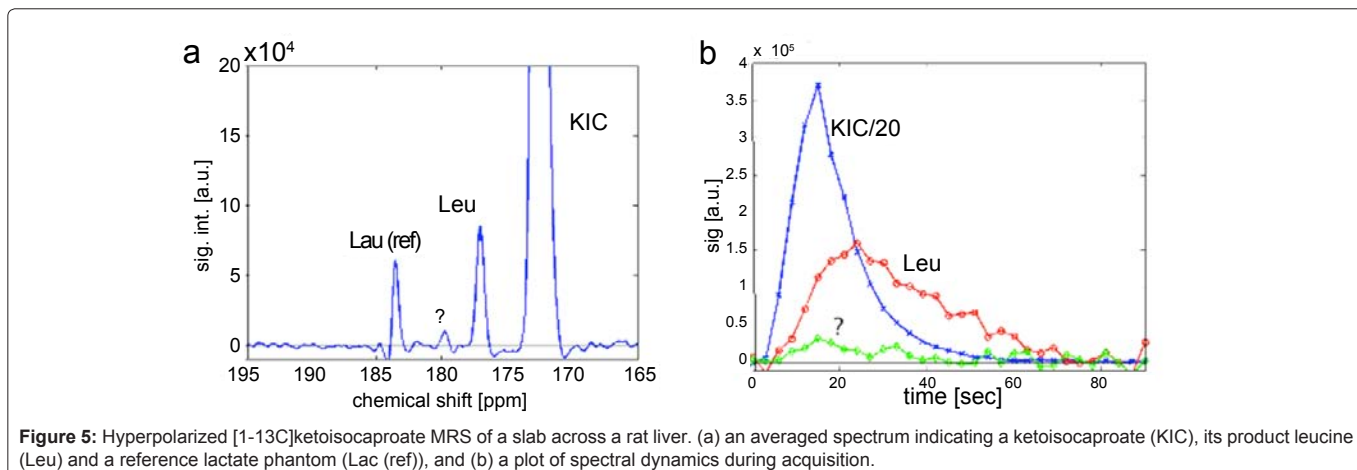


Figure 5: Hyperpolarized [1- ^{13}C]ketoisocaproate MRS of a slab across a rat liver. (a) an averaged spectrum indicating a ketoisocaproate (KIC), its product leucine (Leu) and a reference lactate phantom (Lac (ref)), and (b) a plot of spectral dynamics during acquisition.

modeling tools to measure enzyme kinetics characterizing the *in vivo* metabolism of hyperpolarized [^{1-¹³C}]pyruvate will be essential to the application of the technique with validation by molecular analysis of metabolites and enzymes in liver tissues.

In summary, the objective of this report has been to describe potential molecular hallmarks of an orthotopic hepatocellular carcinoma *in vivo*. The reports herein suggest that the conversion of exogenous [^{1-¹³C}]pyruvate to [^{1-¹³C}]lactate and [^{1-¹³C}]alanine is a characteristic marker of this HCC type *in vivo*. Coupled to this finding, the associated enzymes (*LDH-A*, *NQO1*, and *ALT*) are significantly elevated in this HCC tumor as compared to normal liver that can be detected with non-invasive imaging. Concomitant up-regulation of the enzymes (*LDH-A*, *ALT*, *NQO1*) may explain the observed increases in metabolic products in HCCs, or at least in the HCC type (s) described in this report. In addition, *in vivo* KIC conversion to leucine could be associated with *BCAT-1* and *BCAT-2* expression levels. Such molecular signatures of HCCs could provide an impetus to developing novel enzyme inhibitors as therapeutic agents. Hyperpolarized ¹³C 3D MRSI is a potential diagnostic tool for detection of HCCs and may become an important new imaging tool to measure surrogate markers or endpoints for drug treatment.

Acknowledgements

We very much appreciate the scholarships and critical review of Houry Puzantian, Mona Al Mukaddam and Steven Siegel. We also appreciate the scientific contributions of Yi-Fen Yen, Mei-Sze Chua, Regina H. Clarke-Katzenberg, Dirk Mayer, and, Daniel M. Spielman. Funding sources were provided by the follow NIH grants; KL2RR024132, KL2TR000139, CA09695, RR09784, AA018681, EB009070, AA005965, CA10951; and the T.S. Kwok Foundation. The content of this project is solely the responsibility of the authors and does not necessarily represent the official views of the NIH.

Conflict of Interest

The authors declare that they have no conflict of interest.

References

- Warburg O, Posener K, Negelein E (1924) About the metabolism of the carcinoma cell. *Biochemical Journal* 152: 309-344.
- DeBerardinis RJ (2008) Is cancer a disease of abnormal cellular metabolism? New angles on an old idea. *Genet Med* 10: 767-777.
- Fantin VR, St-Pierre J, Leder P (2006) Attenuation of *LDH-A* expression uncovers a link between glycolysis, mitochondrial physiology, and tumor maintenance. *Cancer Cell* 9: 425-434.
- Plathow C, Weber WA (2008) Tumor Cell Metabolism Imaging. *J Nucl Med* 49: 43S-63S.
- Hirayama A, Kami K, Sugimoto M, Sugawara M, Toki N, et al. (2009) Quantitative Metabolome Profiling of Colon and Stomach Cancer Microenvironment by Capillary Electrophoresis Time-of-Flight Mass Spectrometry. *Cancer Res* 69: 4918-4925.
- Ardenkjaer-Larsen JH, Fridlund B, Gram A, Hansson G, Hansson L, et al. (2003) Increase in signal-to-noise ratio of >10,000 times in liquid-state NMR. *Proc Natl Acad Sci U S A* 100: 10158-10163.
- Albers MJ, Bok R, Chen AP, Cunningham CH, Zierhut ML, et al. (2008) Hyperpolarized ¹³C Lactate, Pyruvate, and Alanine: Noninvasive Biomarkers for Prostate Cancer Detection and Grading. *Cancer Res* 68: 8607-8615.
- Chen AP, Albers MJ, Cunningham CH, Kohler SJ, Yen YF, et al. (2007) Hyperpolarized C-13 spectroscopic imaging of the TRAMP mouse at 3T-initial experience. *Magn Reson Med* 58: 1099-1106.
- Darpolor MM, Yen YF, Chua MS, Xing L, Clarke-Katzenberg RH, et al. (2011) *In vivo* MRSI of hyperpolarized [^{1-¹³C}]pyruvate metabolism in rat hepatocellular carcinoma. *NMR Biomed* 24: 506-513.
- Day SE, Kettunen MI, Gallagher FA, Hu DE, Lerche M, et al. (2007) Detecting tumor response to treatment using hyperpolarized ¹³C magnetic resonance imaging and spectroscopy. *Nat Med* 13: 1382-1387.
- Golman K, Zandt RI, Lerche M, Pehrson R, Ardenkjaer-Larsen JH (2006) Metabolic imaging by hyperpolarized ¹³C magnetic resonance imaging for *in vivo* tumor diagnosis. *Cancer Res* 66: 10855-10860.
- Kettunen MI, Hu DE, Witney TH, McLaughlin R, Gallagher FA, et al. (2010) Magnetization transfer measurements of exchange between hyperpolarized [^{1-¹³C}]pyruvate and [^{1-¹³C}]lactate in a murine lymphoma. *Magn Reson Med* 63: 872-880.
- Park I, Larson PE, Zierhut ML, et al. (2010) Hyperpolarized ¹³C magnetic resonance metabolic imaging: application to brain tumors. *Neuro Oncol* 12: 133-144.
- Ward CS, Venkatesh HS, Chaumeil MM, Brandes AH, Vancracking M, et al. (2010) Noninvasive detection of target modulation following phosphatidylinositol 3-kinase inhibition using hyperpolarized ¹³C magnetic resonance spectroscopy. *Cancer Res* 70: 1296-1305.
- Yen YF, Le Roux P, Mayer D, King R, Spielman D, et al. (2010) T(2) relaxation times of (¹³C) metabolites in a rat hepatocellular carcinoma model measured *in vivo* using (¹³C)-MRS of hyperpolarized [^{1-¹³C}]pyruvate. *NMR Biomed* 23: 414-423.
- Gallagher FA, Kettunen MI, Day SE, Hu DE, Ardenkjaer-Larsen JH, et al. (2008) Magnetic resonance imaging of pH *in vivo* using hyperpolarized ¹³C-labelled bicarbonate. *Nature* 453: 940-943.
- Keshari KR, Wilson DM, Chen AP, Bok R, Larson PE, et al. (2009) Hyperpolarized [^{2-¹³C}]fructose: a hemiketal DNP substrate for *in vivo* metabolic imaging. *J Am Chem Soc* 131: 17591-17596.
- Gallagher FA, Kettunen MI, Hu DE, Jensen PR, Zandt RI, et al. (2009) Production of hyperpolarized [^{1,4-¹³C}]malate from [^{1,4-¹³C}]fumarate is a marker of cell necrosis and treatment response in tumors. *Proc Natl Acad Sci U S A* 106: 19801-19806.
- Karlsson M, Jensen PR, in 't Zandt R, Gisselsson A, Hansson G, et al. (2010) Imaging of branched chain amino acid metabolism in tumors with hyperpolarized ¹³C ketoisocaproate. *Int J Cancer* 127: 729-736.
- Hu S, Chen AP, Zierhut ML, Bok R, Yen YF, et al. (2009) *In vivo* carbon-13 dynamic MRS and MRSI of normal and fasted rat liver with hyperpolarized ¹³C-pyruvate. *Mol Imaging Biol* 11: 399-407.
- Spielman DM, Mayer D, Yen YF, Tropp J, Hurd RE, et al. (2009) *In vivo* measurement of ethanol metabolism in the rat liver using magnetic resonance spectroscopy of hyperpolarized [^{1-¹³C}]pyruvate. *Magn Reson Med* 62: 307-313.
- Hu S, Balakrishnan A, Bok RA, Anderton B, Larson PE, et al. (2011) ¹³C-pyruvate imaging reveals alterations in glycolysis that precede c-Myc-induced tumor formation and regression. *Cell Metab* 14: 131-142.
- Cairns RA, Harris IS, Mak TW (2011) Regulation of cancer cell metabolism. *Nat Rev Cancer* 11: 85-95.
- Reynolds RD, Morris HP (1979) Effects of dietary vitamin B6 on the *in vitro* inactivation of rat tyrosine aminotransferase in host liver and Morris hepatomas. *Cancer Res* 39: 2988-2994.
- Shonk CE, Morris HP, Boxer GE (1965) Patterns of glycolytic enzymes in rat liver and hepatoma. *Cancer Res* 25: 671-676.
- Parkin DM, Bray F, Ferlay J, Pisani P (2005) Global cancer statistics, 2002. *CA Cancer J Clin* 55: 74-108.
- Altekruse SF, McGlynn KA, Reichman ME (2009) Hepatocellular carcinoma incidence, mortality, and survival trends in the United States from 1975 to 2005. *J Clin Oncol* 27: 1485-1491.
- Kim SY, Lee PY, Shin HJ, Kim do H, Kang S, et al. (2009) Proteomic analysis of liver tissue from HBx-transgenic mice at early stages of hepatocarcinogenesis. *Proteomics* 9: 5056-5066.
- Mas VR, Maluf DG, Archer KJ, Yanek K, Bornstein K, et al. (2009) Proteomic analysis of HCV cirrhosis and HCV-induced HCC: identifying biomarkers for monitoring HCV-cirrhotic patients awaiting liver transplantation. *Transplantation* 87: 143-152.
- Yen YF, Kohler SJ, Chen AP, Tropp J, Bok R, et al. (2009) Imaging

- considerations for in vivo ¹³C metabolic mapping using hyperpolarized ¹³C-pyruvate. *Magn Reson Med* 62: 1-10.
31. Mayer D, Yen YF, Takahashi A, Josan S, Tropp J, et al. (2011) Dynamic and high-resolution metabolic imaging of hyperpolarized [¹⁻¹³C]-pyruvate in the rat brain using a high-performance gradient insert. *Magn Reson Med* 65: 1228-1233.
 32. Chen X, Cheung ST, So S, Fan ST, Barry C, et al. (2002) Gene expression patterns in human liver cancers. *Mol Biol Cell* 13: 1929-1939.
 33. Pérez-Villaseñor G, Tovar AR, Moranchel AH, Hernández-Pando R, Hutson SM, et al. (2005) Mitochondrial branched chain aminotransferase gene expression in AS-30D hepatoma rat cells and during liver regeneration after partial hepatectomy in rat. *Life Sci* 78: 334-339.
 34. Ko YH, Pedersen PL, Geschwind JF (2001) Glucose catabolism in the rabbit VX2 tumor model for liver cancer: characterization and targeting hexokinase. *Cancer Lett* 173: 83-91.
 35. Mathupala SP, Ko YH, Pedersen PL (2006) Hexokinase II: cancer's double-edged sword acting as both facilitator and gatekeeper of malignancy when bound to mitochondria. *Oncogene* 25: 4777-4786.
 36. Mathupala SP, Ko YH, Pedersen PL (2009) Hexokinase-2 bound to mitochondria: Cancer's stygian link to the "Warburg effect" and a pivotal target for effective therapy. *Semin Cancer Biol* 19: 17-24.
 37. Pedersen PL (2007) The cancer cell's "power plants" as promising therapeutic targets: an overview. *J Bioenerg Biomembr* 39: 1-12.
 38. Pedersen PL (2007) Warburg, me and Hexokinase 2: Multiple discoveries of key molecular events underlying one of cancers' most common phenotypes, the "Warburg Effect", i.e., elevated glycolysis in the presence of oxygen. *J Bioenerg Biomembr* 39: 211-222.
 39. Chen Z, Zhang H, Lu W, Huang P (2009) Role of mitochondria-associated hexokinase II in cancer cell death induced by 3-bromopyruvate. *Biochim Biophys Acta* 1787: 553-560.
 40. S. Mouli, J. Chung, A.C. Eifler, R.J. Lewandowski, et al. (2010) Image-guided nanoembolization to target microRNA 210 in the VX2 rabbit model of liver cancer. *J Vasc Interv Radiol* 21: S29.
 41. Choi YH, Chung JW, Son KR, So YH, Kim W, et al. (2011) Novel intraarterial therapy for liver cancer using ethylbromopyruvate dissolved in an iodized oil. *Acad Radiol* 18: 471-478.
 42. Soga T, Igarashi K, Ito C, Mizobuchi K, Zimmermann HP, et al. (2009) Metabolomic profiling of anionic metabolites by capillary electrophoresis mass spectrometry. *Anal Chem* 81: 6165-6174.
 43. Hermann HP, Arp J, Pieske B, Kögler H, Baron S, et al. (2004) Improved systolic and diastolic myocardial function with intracoronary pyruvate in patients with congestive heart failure. *Eur J Heart Fail* 6: 213-218.
 44. Hermann HP, Pieske B, Schwarz Müller E, Keul J, Just H, et al. (1999) Haemodynamic effects of intracoronary pyruvate in patients with congestive heart failure: an open study. *Lancet* 353: 1321-1323.

Author Affiliations


Top

¹Departments of Radiology, University of Pennsylvania, Philadelphia, PA, USA

²Departments of Gastroenterology, University of Pennsylvania, Philadelphia, PA, USA

³Departments of Biological Chemistry and Oncology, Sidney Kimmel Cancer Research Center, and Center for Obesity Research & Metabolism, John Hopkins University, School of Medicine, Baltimore, MD, USA

Submit your next manuscript and get advantages of SciTechnol submissions

- ❖ 50 Journals
- ❖ 21 Day rapid review process
- ❖ 1000 Editorial team
- ❖ 2 Million readers
- ❖ More than 5000 
- ❖ Publication immediately after acceptance
- ❖ Quality and quick editorial, review processing

Submit your next manuscript at • www.scitechnol.com/submission